English Channel Winter Storminess Has Increased to Levels Last Seen 200 Years Ago

Supplementary Information

Richard C. Cornes[1] and Philip D. Jones[2]

[1]National Oceanography Centre, Southampton, UK
[2]Climatic Research Unit, School of Environmental Sciences, University of East Anglia, Norwich, UK

S1 Uncertainty in the Early Pressure Data

In his evaluation of the geostrophic wind triangle technique for estimating wind speed trends, Lindau (2006) demonstrated that random uncertainties in the three pressure series leads to systematic biases in the geowind series. Lindau showed that the geostrphic wind speed calculated using a triple of MSLP is equivalent to the variance (V) across the three observations $V = \frac{a^2}{4g^2}$, where a is the distance between observations (based on a simplified situation where the triangle is equilateral) and g is the horizontal pressure gradient $g^2 = (\frac{dp}{dx})^2 + (\frac{dp}{dy})^2$. V clearly varies with the magnitude of the pressure gradient but random uncertainty in the values of p also lead to an increase in V.

Lindau's analysis was restricted to MSLP values taken onboard merchant ships, which were estimated to have a random uncertainty magnitude of 2–3hPa. Expressing V as a standard deviation:

$$\sigma_p = \frac{a}{2g} \tag{1}$$

An appropriate value of a was given by Lindau as 200km; beyond that distance the method cannot be applied because the fields are no longer linear. The typical pressure gradient is 10-3 Pa m-1 giving typical standard deviations (σ_p) of 1hPa. However, as the magnitude of this variance is a half to one-third the size of the random uncertainty of 2-3hPa, and the geowind variance or signal becomes obscured by the variance due to uncertainty in the measurements.

A question that arises from this analysis with regard to the London-Paris-De Bilt pressure triangle is: does the increase geostrophic wind values in the early part of the series arise from random uncertainty associated with the MSLP observations? Manley (1964) estimated the MSLP values that he derived in the

London Weather Diary to be true to the nearest 1hPa, or alternatively the random uncertainty was ±0.5hPa. This relates to the measurement precision of the barometers of 1/100ths English inch (which equals 0.3hPa) plus additional random uncertainty components related to the other adjustments for temperature and altitude. This 1hPa random uncertainty, taking Lindau's order of magnitude analysis, is an equivalent value to the expected variance across the idealized equilateral triangle. However, the distance between the observations in the London-Paris-De Bilt triangle is also slightly larger than the 200km used by Lindau, and is around 300km. As such the pressure gradient variance σ_p is the order of 1.5hPa. In this case, therefore, the signal is not obscured by the random uncertainty in MSLP values that has been seen in the ship observations by Lindau.

Another feature of the London-Paris-De Bilt pressure triangle series that might suggest an increase geostrophic wind values as a result of random MSLP uncertainties is the increase across the year, rather than in any particular season. However, as has been demonstrated in the main paper, this feature is also seen in the storm frequency series taken from the weather diaries kept at Armagh Observatory. In addition a reduction in storm frequency after ca. 1830 is also seen in that storm series, and of a similar magnitude as seen in the geostrophic wind results. While the Armagh series has deficiencies in examining multi-century changes in storm frequency as a result of the change in recording practice in the later nineteenth century, the series during this early period a considered a reliable, independent comparison to the pressure triangle results.

A further piece of information from the geostrophic wind series that suggests that the increase in storminess in the early part of the record is a true feature of the long-term trends in storminess comes from the separation of the U and V components (Figs. S1 and S2). A spurious increase in variance in the pressure series as a result of random uncertainty would be expected to lead to an increase in both U and V components. However, this is not apparent in the data and the time series indicate no breakpoints throughout the early part of the series. A long-term trend in the V component, towards more southern conditions, is evident these data as described in the main paper.

S2 Station-based Storm Indices

Several previous studies have analysed changes in storminess using station-based indices calculated using MSLP series (e.g. Bärring and Fortuniak, 2009). We have calculated a selection of such indices using the three MSLP series and these are plotted in figures S7 to S14 at the seasonal and annual resolution.

The first thing that is observed in these plots that there is generally no long-term trend in the data, in contrast to the clear signal that is observed in the geostrophic wind speed series that has been derived from these data. Related to this is the high-degree of interannual variability in these station-level indices, which makes the detection of significance in any trend difficult to achieve.

One feature that is apparent in the indices that use a day-to-day difference in pressure to define storminess (Figs. S9–S12) is the subdued values before ca. 1774 in the London series, and particularly for the period 17ZZ–17XX. Reduced values are also seen during this period in the other two but not to the degree seen in the London data. It is likely that this is due to a propoensity for the barometers used at that time to stick. In the geostrophic wind series this deficiency in the data will become most apparent during the summer months when the pressure gradients tend to be low and likely results in the exceptionally high rate of storminess seen at that time in Fig. 1 of the main paper. Although it also occurs in the winter season, the higher pressure gradients during that season tends to mask the effect.

S3 Comparing Sampling Frequencies

In Fig. S6 we have plotted percentiles of geowind calculated using the noon-only values (as used in the main paper) and similar percentiles calculated using three-hourly data for ther period 1950–2022. Two features are apparent when comparing the two sets of results: firstly the uncertainty is much larger in the noon-only data, which is due to the much smaller number of values from which the percentiles are calculated; and secondly the low-frequency variability is broadly comparable between the sampling frequencies.

References

Bärring, L. and Fortuniak, K. (2009). Multi-indices analysis of southern Scandinavian storminess 1780-2005 and links to interdecadal variations in the NW Europe-North Sea region. *International Journal of Climatology*, 29(3):373–384.

Lindau, R. (2006). The Elimination of spurious trends in marine wind data using pressure observations. *International Journal of Climatology*, 26(6):797–817.

Manley, G. (1964). London Weather Diary. Unpublished manuscript. Copy of the original., Climatic Research Unit Library, University of East Anglia.

S4 Supplementary Figures

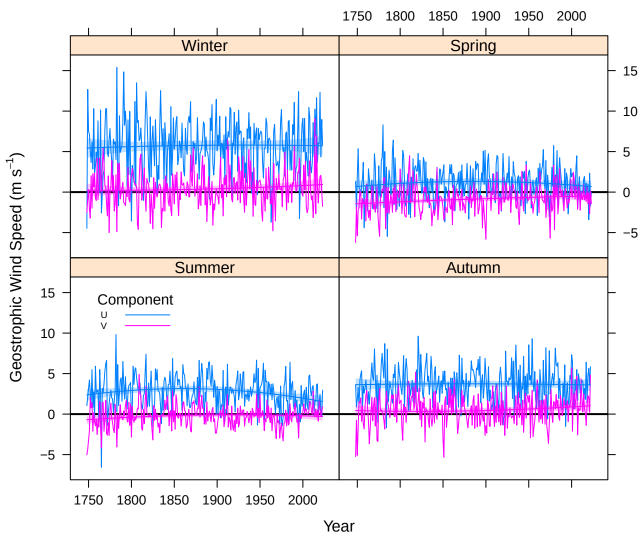

Figure S1: Median U and V wind components calculated for each season over the period 1747–2023.

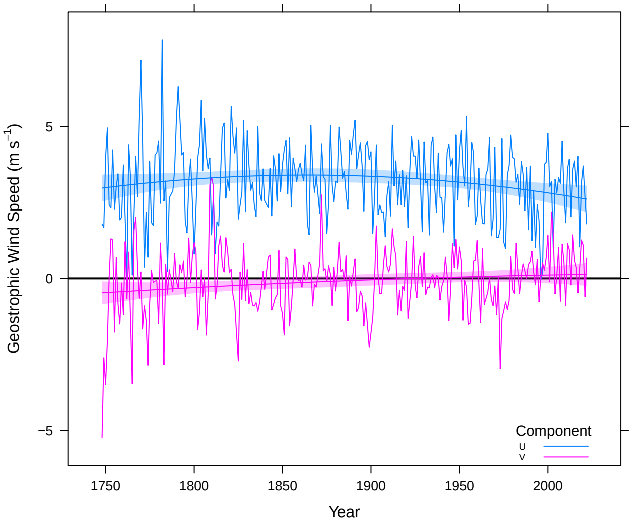

Figure S2: As Figure S1 but for annual values.

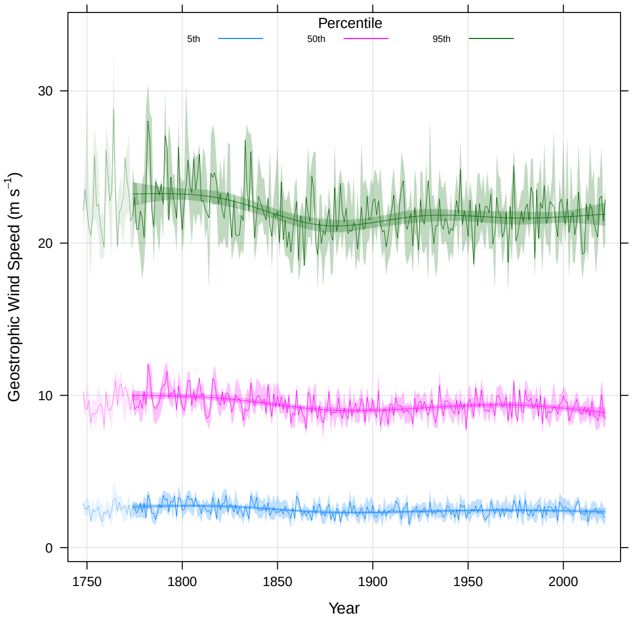

Figure S3: As Figure 1b in the main text but calculating the percentiles using annual geostrophic wind-speed values.

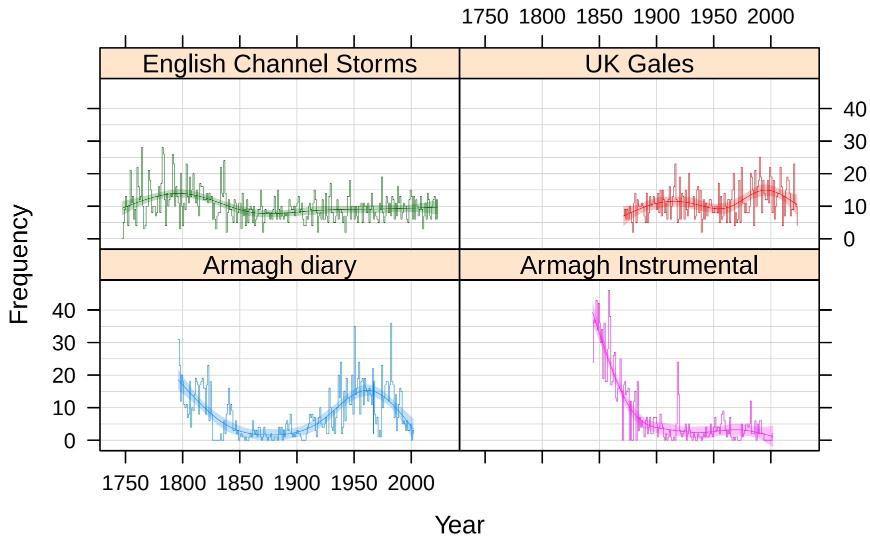

Figure S4: As Fig. 2 in the main text but at the annual resolution.

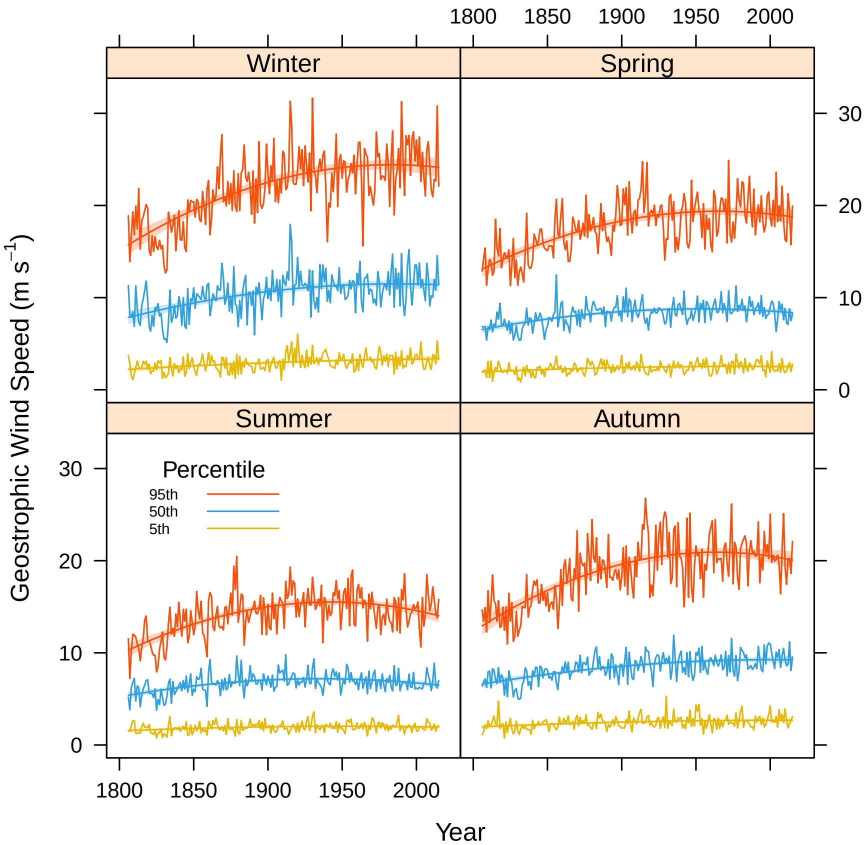

Figure S5: Geostrophic wind speed percentiles per season calculated from the the ensemble mean from the 20CRv3 dataset using noon values (1806–2015).The wind-speed values are calculated using the same method as for the L-P-D triangle series but using the grid-cell values nearest to the three sites.

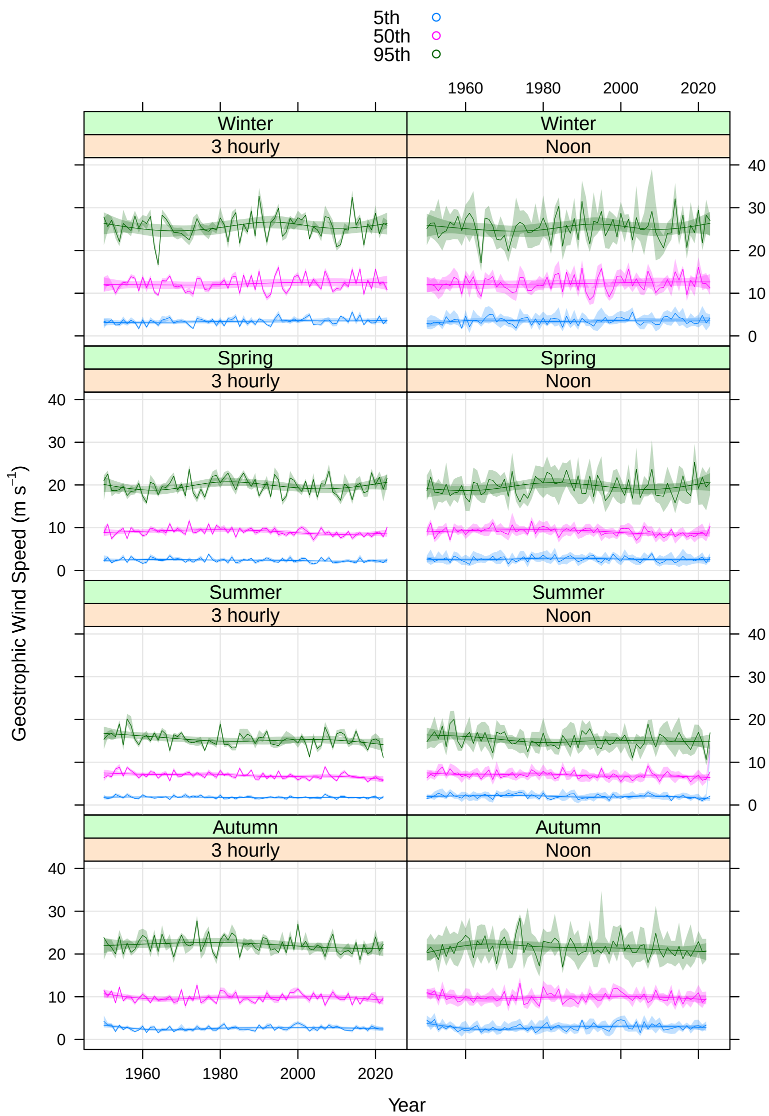

Figure S6: Seasonal percentiles of geostrophic wind speed percentiles calculated using noon values (right column) and three-hourly (left column) pressure values over the period 1950–2023. Uncertainty values are calculated as described in the Methods section of the main text.

a) n1005

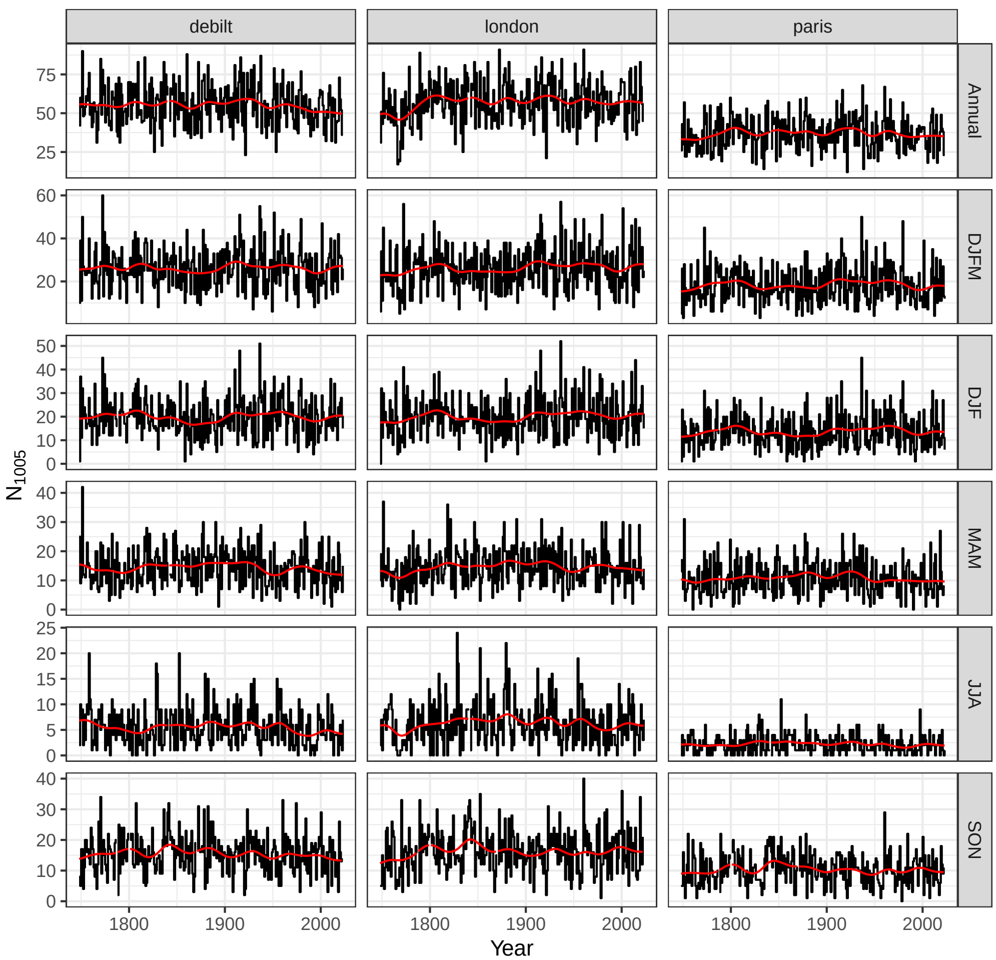

Figure S7: Time series (1747–2023) of the number of days where pressure is less than 1005hPa in the three pressure series at the annual and seasonal resolutions. Note the differnt scales on the y-axes.

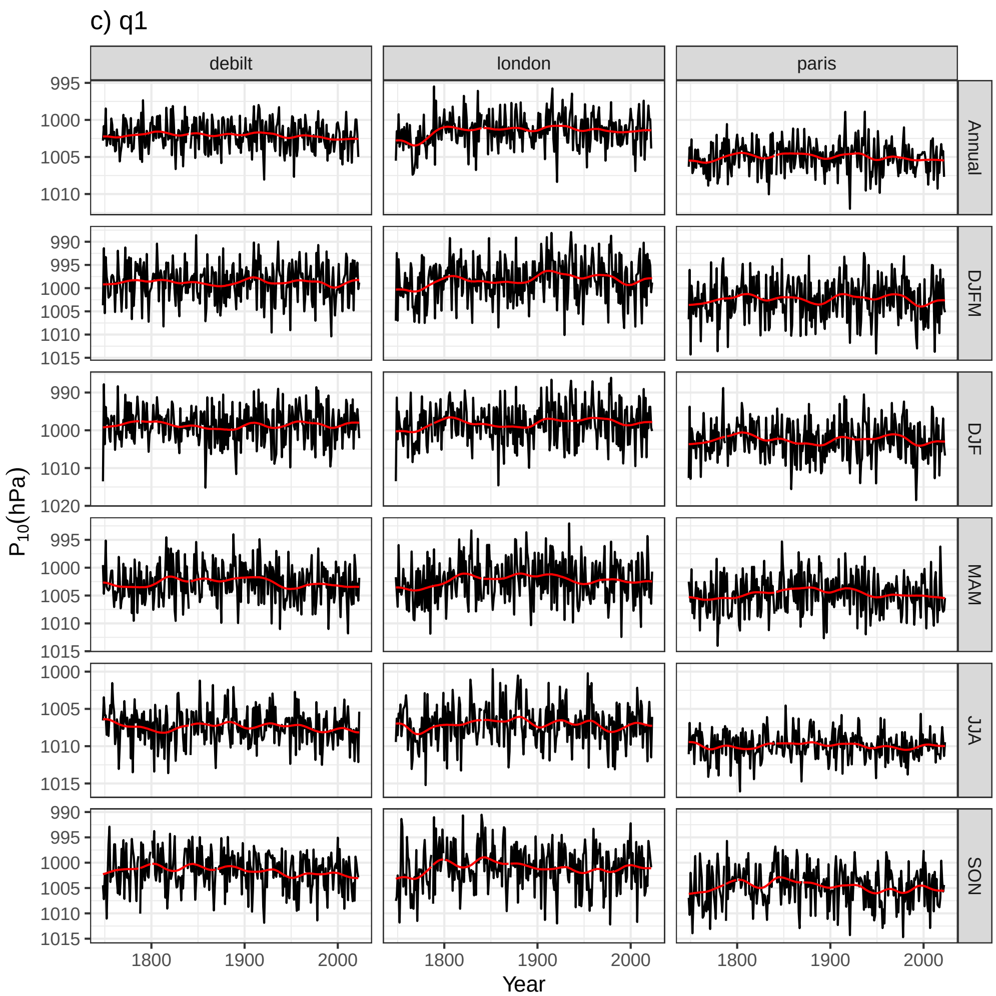

Figure S8: As Figure S7 but for the lower quantile of MSLP.

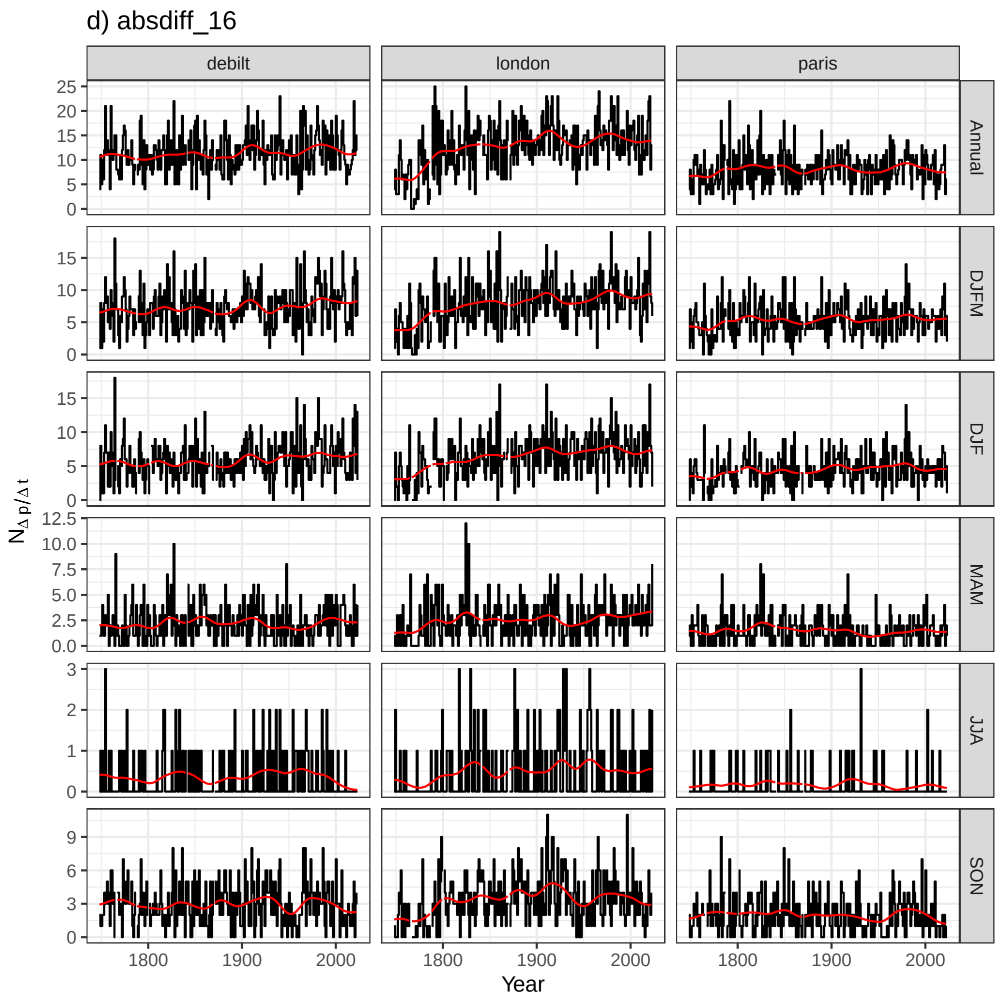

Figure S9: As Figure S7 but for absolute daily difference in pressure over 16hPa.

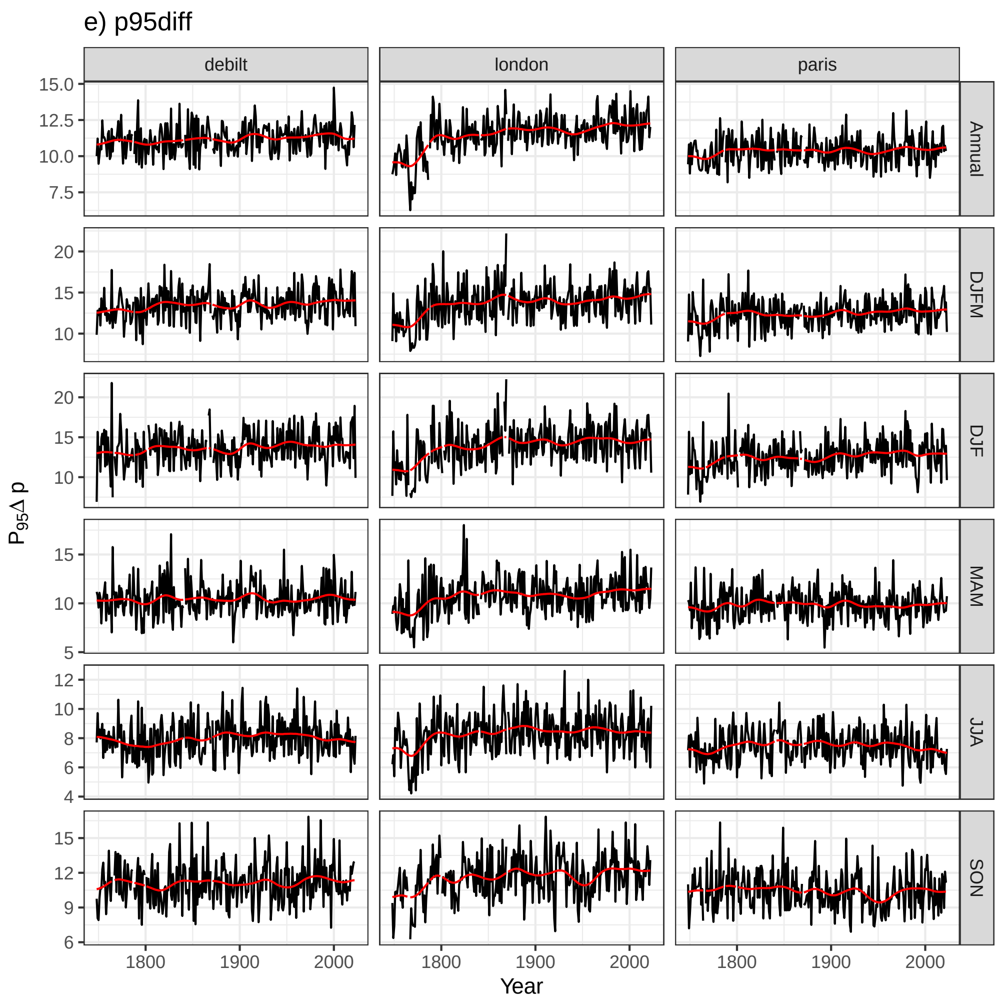

Figure S10: As Figure S7 but for the 95th percentile in absolute daily pressure differences.

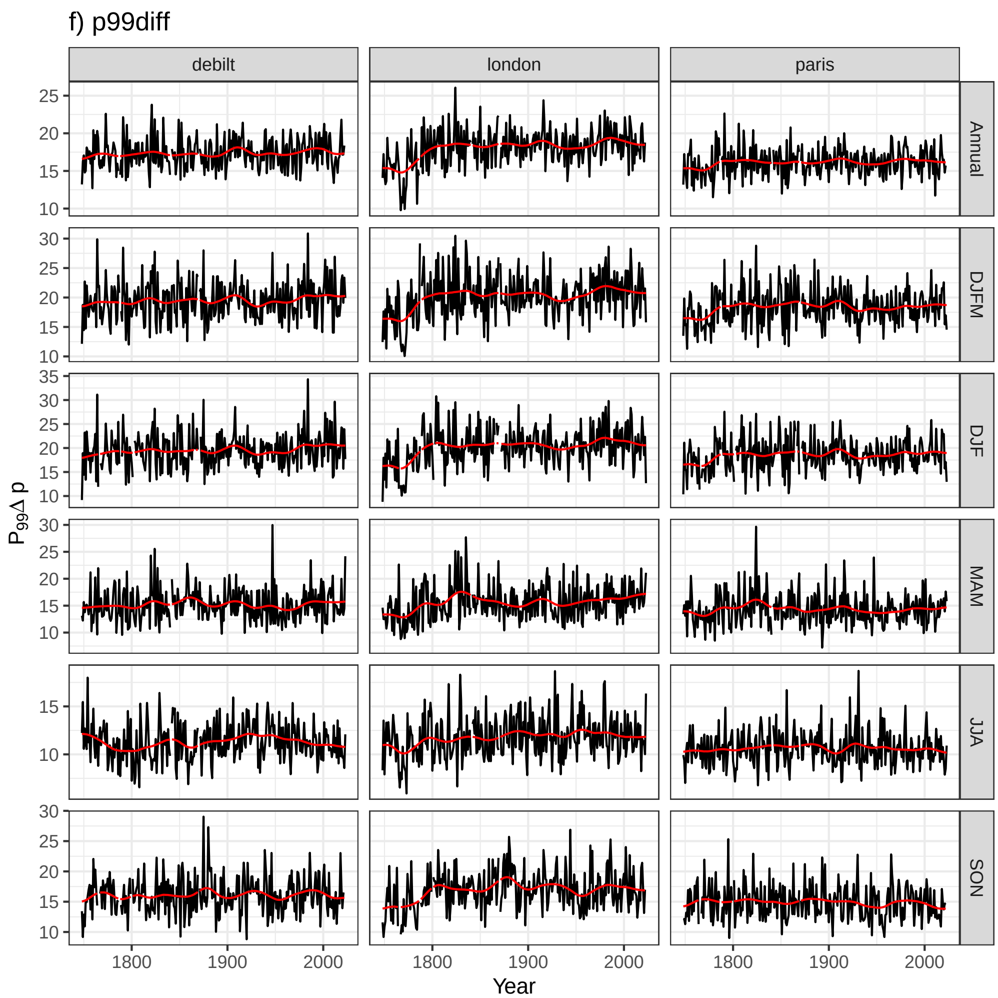

Figure S11: As Figure S7 but for the 99th percentile in absolute daily pressure differences.

g) mndiff

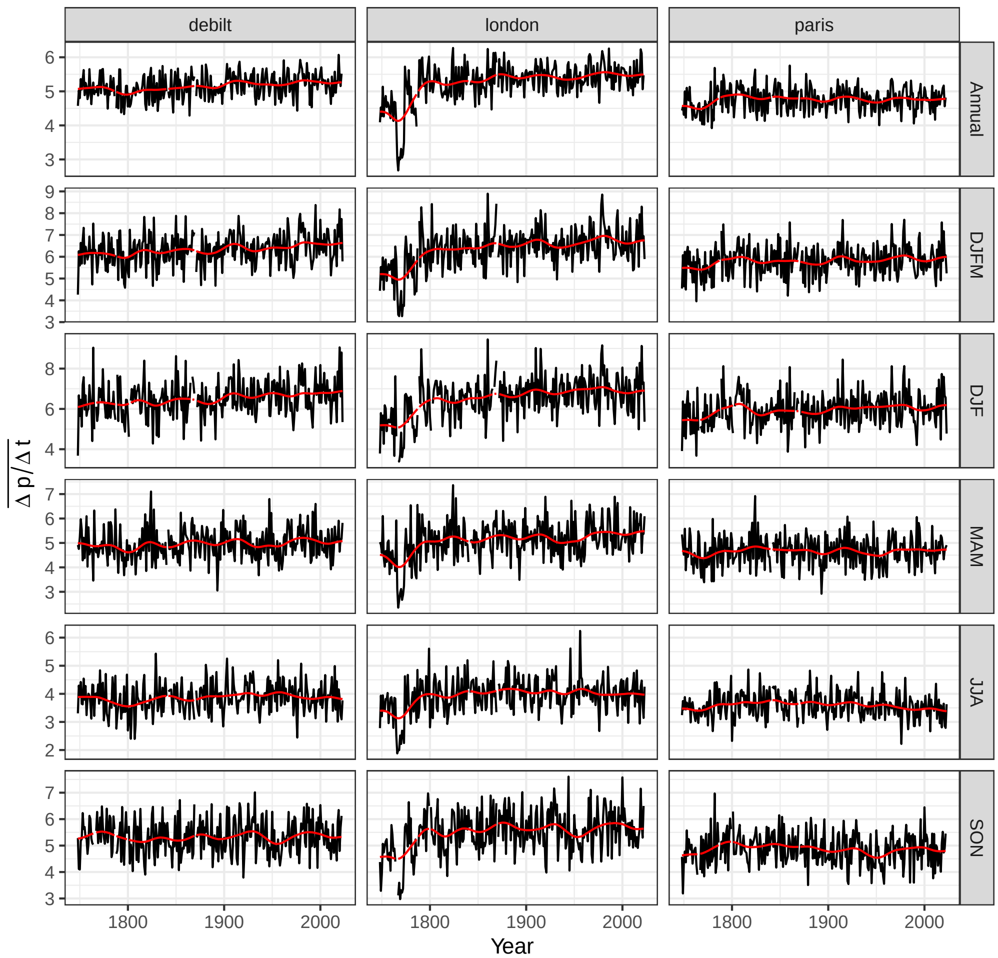

Figure S12: As Figure S7 but for the mean absolute daily pressure differences.

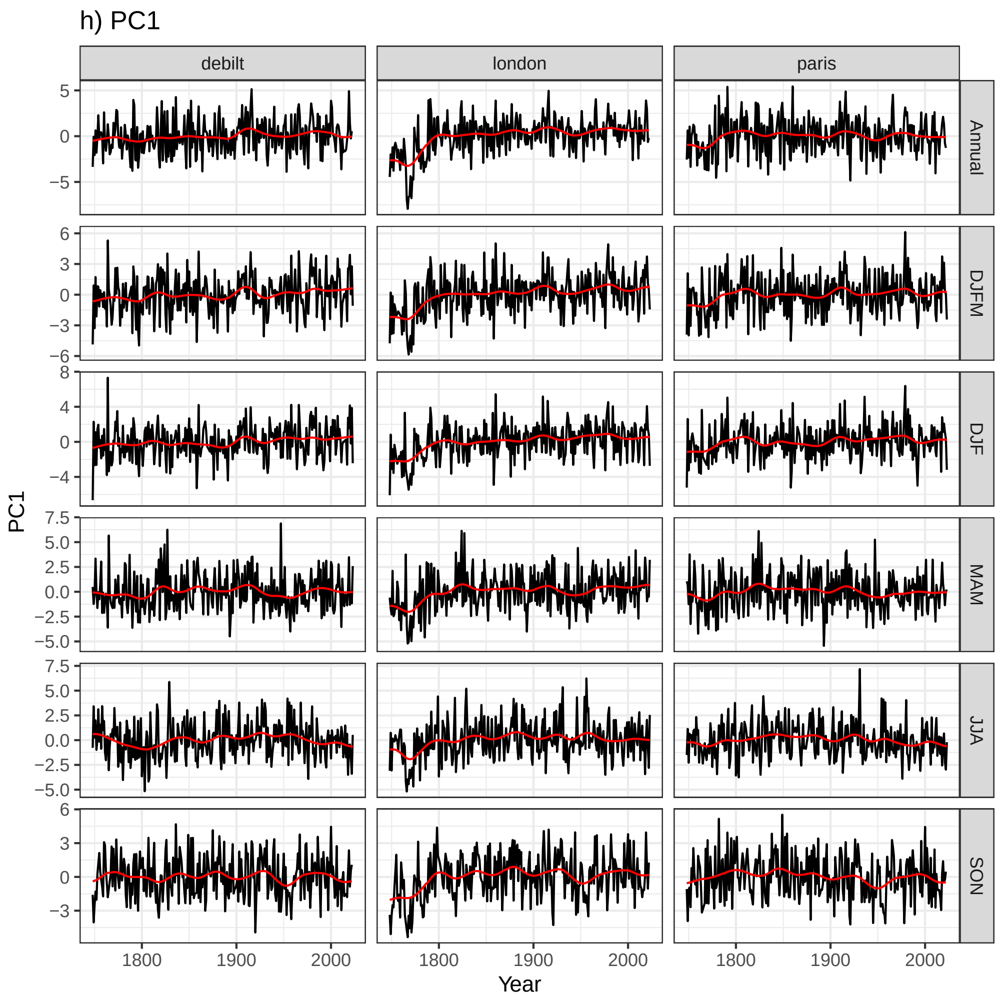

Figure S13: As Figure S7 but for the leading principal component.

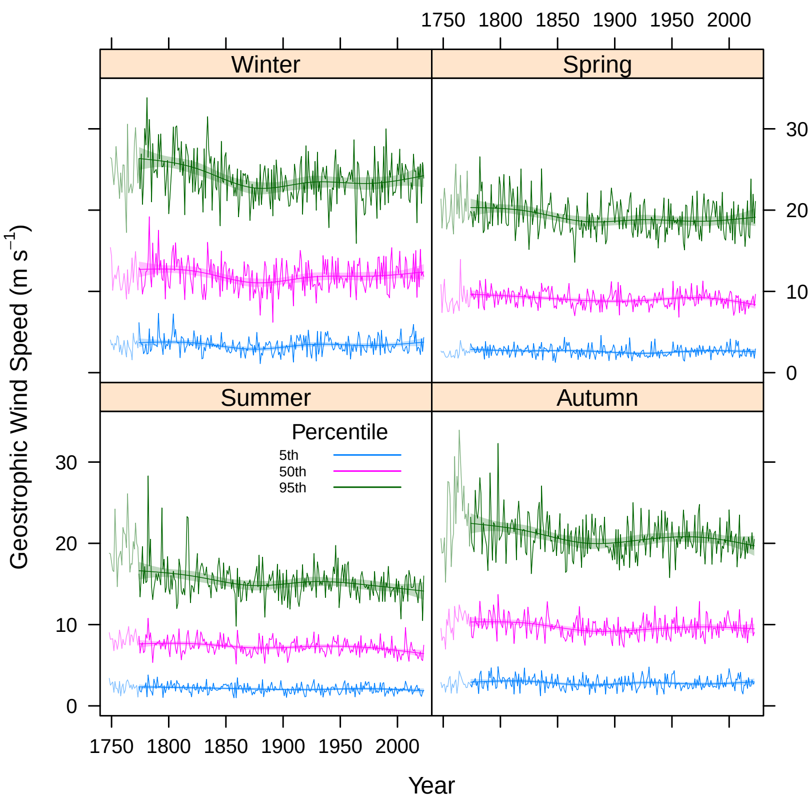

Figure S14: As Figure 2b in the main text but using London sub-sampled to only a 9am (±2 hour) value.

S5 Supplementary Tables

Date	debilt	london	paris	G	U	V	Direction
1990-01-25	983.20	972.60	995.00	47.69	37.77	29.12	232.38
1993-11-14	992.60	1013.70	1015.70	46.32	26.02	-38.31	325.81
2020-02-09	998.60	989.80	1011.10	45.02	37.23	25.31	235.79
1987-03-27	990.30	980.50	1000.60	42.89	33.60	26.66	231.57
1982-12-19	1001.10	990.50	1010.00	42.05	31.47	27.89	228.45
2008-01-15	992.40	979.50	997.80	41.29	26.50	31.65	219.94
1992-11-11	978.80	997.00	1000.10	41.24	25.43	-32.47	321.93
2007-01-18	984.70	988.30	1005.50	41.07	41.07	0.57	269.20
1990-12-26	997.10	987.00	1006.00	40.87	30.90	26.75	229.11
2008-01-31	1007.10	1000.90	1020.10	40.41	35.34	19.60	240.99

Table S1: Top ten storms ranked by values of the geostrophic wind speed (G) over the period January 1979- December 2023 from the 12pm daily geostrophic wind series. Also indicated are the MSLP values at the three sites, the U and V wind vectors and the direction of geostrophic wind (direction).

season	quantile	trend	lbound	ubound
Summer	50th	-0.42	-0.72	-0.09
Summer	5th	-0.10	-0.29	0.10
Summer	90th	-0.71	-1.26	-0.13
Summer	95th	-0.55	-1.21	0.11
Summer	99th	-0.84	-1.82	0.11
Autumn	50th	0.39	-0.04	0.82
Autumn	5th	0.12	-0.14	0.39
Autumn	90th	0.23	-0.46	0.95
Autumn	95th	-0.21	-1.13	0.67
Autumn	99th	-0.70	-1.82	0.40
Winter	50th	0.92	0.22	1.64
Winter	5th	0.51	0.16	0.84
Winter	90th	0.96	0.11	1.87
Winter	95th	1.12	0.15	2.08
Winter	99th	0.71	-0.67	2.18
Spring	50th	-0.10	-0.44	0.24
Spring	5th	0.17	-0.08	0.40
Spring	90th	-0.29	-0.89	0.31
Spring	95th	0.08	-0.72	0.87
Spring	99th	0.06	-1.22	1.33

Table S2: Trends in seasonal geostrophic wind percentiles over the period 1871–2022. The 95th uncertainty range is indicated by the lbound and ubound columns

season	quantile	trend	lbound	ubound
Summer	50th	-0.51	-0.65	-0.37
Summer	5th	-0.15	-0.24	-0.06
Summer	90th	-0.93	-1.22	-0.64
Summer	95th	-0.98	-1.37	-0.60
Summer	99th	-1.26	-1.83	-0.71
Autumn	50th	-0.32	-0.54	-0.11
Autumn	5th	-0.06	-0.18	0.05
Autumn	90th	-0.38	-0.74	-0.06
Autumn	95th	-0.65	-1.08	-0.19
Autumn	99th	-0.58	-1.22	0.05
Winter	50th	-0.03	-0.34	0.29
Winter	5th	0.05	-0.12	0.20
Winter	90th	-0.19	-0.61	0.23
Winter	95th	-0.24	-0.69	0.24
Winter	99th	-0.41	-1.05	0.21
Spring	50th	-0.11	-0.26	0.05
Spring	5th	-0.03	-0.13	0.06
Spring	90th	-0.44	-0.74	-0.17
Spring	95th	-0.46	-0.80	-0.08
Spring	99th	-0.99	-1.58	-0.37

Table S3: As Table S2 except for the period 1748-2022.

season	quantile	trend	lbound	ubound
Summer	50th	-1.15	-2.00	-0.34
Summer	5th	-0.64	-1.25	-0.05
Summer	90th	-1.87	-3.46	-0.40
Summer	95th	-1.96	-4.05	0.19
Summer	99th	-1.32	-4.73	2.01
Autumn	50th	-0.25	-1.48	1.00
Autumn	5th	0.63	-0.25	1.57
Autumn	90th	-0.89	-2.76	1.16
Autumn	95th	-1.45	-3.62	0.70
Autumn	99th	-1.46	-4.42	1.59
Winter	50th	1.25	-1.00	3.38
Winter	5th	0.48	-0.55	1.47
Winter	90th	0.94	-2.01	4.04
Winter	95th	0.06	-3.18	3.34
Winter	99th	0.14	-4.23	5.26
Spring	50th	-1.51	-2.55	-0.52
Spring	5th	-0.10	-0.81	0.58
Spring	90th	-0.85	-2.51	1.16
Spring	95th	0.61	-1.73	3.18
Spring	99th	1.85	-1.97	5.95

Table S4: As Table S2 except for the period 1950-2022.

season	pc	3 hourly	Noon
Autumn	5th	0.18 (-0.49 - 0.78)	0.63 (-0.25 - 1.57)
Autumn	50th	-0.14 (-1.35 - 1.18)	-0.25 (-1.48 - 1)
Autumn	95th	-1.84 (-3.86 - 0.29)	-1.45 (-3.62 - 0.7)
Summer	5th	-0.19 (-0.53 - 0.17)	-0.6 (-1.2 - -0.02)
Summer	50th	-1.7 (-2.56 - -0.9)	-1.01 (-1.92 - -0.2)
Summer	95th	-2.23 (-4 - -0.33)	-1.5 (-3.43 - 0.44)
Spring	5th	-0.43 (-1 - 0.03)	-0.04 (-0.74 - 0.63)
Spring	50th	-1.19 (-2.18 - -0.21)	-1.4 (-2.4 - -0.38)
Spring	95th	0.54 (-1.9 - 2.66)	0.73 (-1.62 - 3.3)
Winter	5th	0.72 (-0.13 - 1.59)	0.55 (-0.48 - 1.49)
Winter	50th	0.96 (-1.05 - 3.08)	0.96 (-1.09 - 3.12)
Winter	95th	0.43 (-2.29 - 3.07)	0.23 (-2.86 - 3.44)

Table S5: Linear trends and 95pctile uncertainty range of the seasonal L-P-Dtri time series over the period 1950-2021 using noon-only and three–hourly sampling.

pc	Autumn	Summer	Spring	Winter
5th	0.66	0.51	0.55	0.67
50th	0.86	0.87	0.86	0.94
95th	0.72	0.79	0.80	0.79

Table S6: Linear regression of 3-hourly and noon-only percentiles

pc	Autumn	Summer	Spring	Winter
5th	0.52	0.41	0.48	0.51
50th	0.42	0.30	0.35	0.43
95th	1.25	0.82	0.97	1.29

Table S7: Root, mean-squared error of the noon-only L-P-Dtri season quantiles against the three-hourly sampling series.

jet_stat	pc	estimate	conf.low	conf.high	series
speed	5th	0.36	0.21	0.49	correlation detrended
speed	5th	0.40	0.26	0.53	correlation
speed	50th	0.58	0.46	0.68	correlation detrended
speed	50th	0.61	0.49	0.70	correlation
speed	95th	0.43	0.29	0.56	correlation detrended
speed	95th	0.46	0.32	0.58	correlation
lat	5th	-0.26	-0.40	-0.10	correlation detrended
lat	5th	-0.24	-0.39	-0.08	correlation
lat	50th	-0.06	-0.22	0.11	correlation detrended
lat	50th	-0.04	-0.20	0.12	correlation
lat	95th	0.11	-0.05	0.27	correlation detrended
lat	95th	0.12	-0.04	0.28	correlation

Table S8: Correlations between Jet Parameters and Geowind Statistics

season	pc	EA	NAO_EOF	NAO_HUR
Winter	95th	0.27*	0.43**	0.39**
Winter	50th	0.34**	0.38**	0.33**
Winter	5th	0.17	0.02	-0.01
Spring	95th	0.05	0.15	0.18
Spring	50th	-0.12	-0.13	-0.11
Spring	5th	0.07	-0.1	-0.13
Summer	95th	-0.04	-0.37**	-0.07
Summer	50th	-0.27*	-0.32**	-0.18
Summer	5th	-0.17	-0.28*	-0.08
Autumn	95th	0.15	-0.1	0.16
Autumn	50th	0.17	-0.13	0.14
Autumn	5th	0.08	-0.21	0.02

Table S9: Correlation between the geowind percentiles per season and three teleconnection indices over the period 1950-2022: EA - East Atlantic Pattern (`https://www.cpc.ncep.noaa.gov/data/teledoc/ea.shtml`); NAO_HUR - Hurrell NAO index (`https://climatedataguide.ucar.edu/climate-data/hurrell-north-atlantic-oscillation-nao-index-station-based`); NAO_EOF - Index Derived from the leading EOF of 500 millibar height field over 0-90N (`https://www.ncdc.noaa.gov/teleconnections/nao/`). * indicates correlations signficant at $p < 0.05$; ** indicates correlations significant at $p < 0.01$